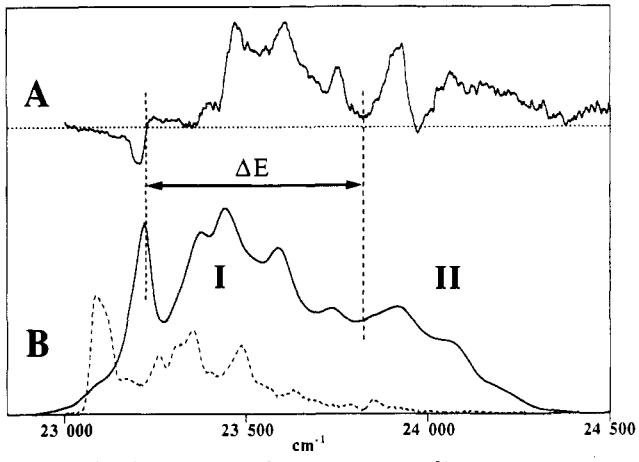

Figure 4. $^4A_{1g}{}^4E_g$ region (Mn^{2+}) in $MnBr_2$:5%Ti^{2+} at 4.2 K: (A) MCD spectrum; (B) absorption spectrum (solid line). The dashed line represents the absorption spectrum of pure $MnBr_2$ at 4.2 K with expanded (factor of 5) ordinate scale.

transition on Ti^{2+} is also intraconfigurational, within $(t_{2g})^2$, and thus the double excitations in the Ti^{2+}–Mn^{2+} pairs and Ti^{2+}-$(Mn^{2+})_6$ clusters are also observed as sharp absorption bands. The situation is different for the $^4T_{2g}$ transition in Mn^{2+}. Due to its intrinsic broadness, bands I and II are not resolved and we only observe a blue-shift and an asymmetric shape of the corresponding absorption band; see Figure 1. Note that the $^4T_{1g}$ transition on Mn^{2+} neither is enhanced in $MnCl_2$:Ti^{2+} nor shows a blue-shift. Exchange interactions between Ti^{2+} and Mn^{2+} are evidently much less efficient in inducing intensity for this transition.

(b) $MnBr_2$. The two band systems I and II for the $^4T_{2g}$ and $^4A_{1g}{}^4E_g$ excitations of Mn^{2+} are also observed in the absorption and MCD spectra of $MnBr_2$:Ti^{2+}, but not as clearly separated from each other as in the chlorides. Figure 4 shows the $^4A_{1g}{}^4E_g$ region in comparison with the absorption spectrum of pure $MnBr_2$. The energy separation ΔE, corresponding to the trigonal Ti^{2+} ground-state splitting, is roughly 600 cm^{-1}. In this case, ΔE is not accessible by luminescence spectroscopy, because Ti^{2+} does not show sharp emission lines in bromide lattices.[8]

Conclusion

The principle of coupling an infrared electronic excitation on one ion with a visible excitation on a neighboring ion, thus producing an easily detectable sideband in the absorption spectrum of the latter, should be applicable to many other pairs of ions. The best results can be expected in those cases in which the visible absorption corresponds to a sharp-band intraconfigurational transition.

Acknowledgment. This work was financially supported by the Swiss NSF and the French CNRS.

Registry No. $MnCl_2$, 7773-01-5; $MnBr_2$, 13446-03-2; $MgCl_2$, 7786-30-3; Ti^{2+}, 15969-58-1; Mn^{2+}, 16397-91-4.

Contribution from the Institute for Molecular Science, Myodaiji, Okazaki 444, Japan, and Department of Applied Chemistry, Faculty of Engineering, Osaka University, Yamada-oka, Suita, Osaka 565, Japan

Electrochemical Assimilatory and Dissimilatory Reductions of NO_3^- and NO_2^- via a Possible Free NO Intermediate

Koji Tanaka,*[†] Nobutoshi Komeda,[‡] and Tatsuji Matsui[‡]

Received August 24, 1990

Both NO_3^- and NO_2^- were selectively reduced to NH_3 by a $(Bu_4N)_4[MoFe_3S_4(SPh)_3(O_2C_6Cl_4)]_2$-modified glassy-carbon electrode ($[MoFe_3S_4]$/GC) under controlled-potential electrolysis at −1.25 V vs SCE in H_2O (pH 10.0), while NO_2^- was reduced predominantly to N_2 by the same electrode under electrolysis at −1.00 V. Nitrite ion preferentially binds to molybdenum of the $[MoFe_3S_4]$/GC with the oxygen atom, where either bound or terminal oxygen of the Mo–ONO^- moiety is removed by reduction. An electrochemical study indicates the presence of free NO as the common reaction intermediate in these assimilatory and dissimilatory reductions of NO_2^-.

Introduction

Dissimilatory and assimilatory reductions of NO_3^- and NO_2^- are the key reactions in the nitrogen cycle. Although the details of these enzymatic reductions have not been fully elucidated so far, it is generally believed that NO_3^- is first reduced to NO_2^- by molybdenum-containing nitrate reductases,[1] and then NO_2^- is reduced to NH_3 via nitrosyl and hydroxylamine by assimilatory nitrite reductases containing sirohemes.[2] On the other hand, dissimilatory nitrite reductases containing hemes *c* and d_1[3] reduce NO_2^- to N_2O, which is further reduced to N_2.[4] The N–N bond formation in the dissimilatory reduction of NO_2^- is currently a matter of controversy; generally accepted pathways from NO_2^- to N_2O are either nucleophilic attack of NO_2^- on E-NO^+ generated by an acid–base equilibrium reaction of enzyme-bound NO_2^- (E-NO_2^-)[5] or dimerization of HNO (or NO^-) resulting from two-electron reduction of NO_2^-.[6] Evolution of low levels of NO from nitrite reductases,[7] however, further complicates these pathways since the affinity of heme protein for NO is very strong[8]

[†] Institute for Molecular Science.
[‡] Osaka University.

(1) (a) Payne, W. J. *Denitrification*; Wiley-Interscience: New York, 1981; p 214. (b) Adams, M. W. W.; Mortenson, L. E. *Molybdenum Enzymes*; Spiro, T. G., Ed.; Wiley-Interscience: New York, 1985; pp 519–593.
(2) (a) Vega, J. M.; Kamin, H. *J. Biol. Chem.* **1977**, *252*, 896. (b) Murphy, M. J.; Siegel, L. M.; Tove, S. R.; Kamin, H. *Proc. Natl. Acad. Sci. U.S.A.* **1974**, *71*, 612.
(3) (a) Timkovich, R.; Cork, M. S.; Taylor, P. V. *J. Biol. Chem.* **1984**, *259*, 1577. (b) Timkovich, R.; Dhesi, R.; Martinkus, K. J.; Robinson, M. K.; Rea, T. M. *Arch. Biochem. Biophys.* **1982**, *215*, 47.
(4) Henry, Y.; Bessieres. *Biochimie* **1984**, *66*, 259.
(5) (a) Garber, E. A. E.; Hollocher, T. C. *J. Biol. Chem.* **1982**, *257*, 8091. (b) Weeg-Aerssens, E.; Tiedje, J. M.; Averill, B. A. *J. Am. Chem. Soc.* **1988**, *110*, 6851. (c) Aerssens, E.; Tiedje, J. M.; Averill, B. A. *J. Biol. Chem.* **1986**, *261*, 9652. (d) Averill, B. A.; Tiedje, J. M. *FEBS Lett.* **1982**, *138*, 8.
(6) (a) Kim, C.-H.; Hollocher, T. C. *J. Biol. Chem.* **1984**, *259*, 2092. (b) Garber, E. A. E.; Hollocher, T. C. *J. Biol. Chem.* **1982**, *257*, 4705. (c) Kim, C.-H.; Hollocher, T. C. *J. Biol. Chem.* **1983**, *258*, 4861. (d) Garber, E. A. E.; Wehrli, S.; Hollocher, T. C. *J. Biol. Chem.* **1983**, *258*, 3587.

0020-1669/91/1330-3282$02.50/0

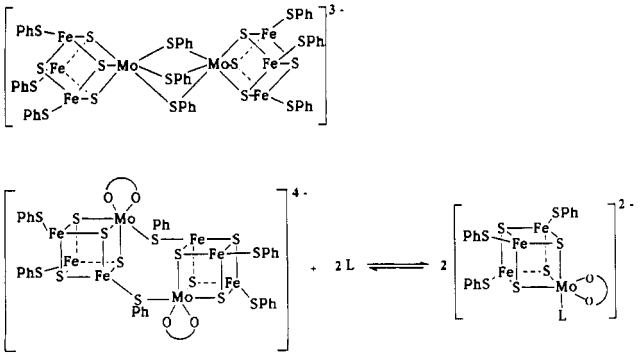

Figure 1. Structures of $[Mo_2Fe_6S_8(SPh)_9]^{3-}$ and $[MoFe_3S_4(SPh)_3(O_2C_6Cl_4)]_2^{4-}$.

and the dissociation of NO from ferrous heme–NO is even slower than CO dissociation.[9]

Much effort has been devoted to the study of electrochemical[10] and photochemical reductions of NO_n^- (n = 2, 3)[11] using homogeneous catalysts with the aim of mimicking these enzymatic reactions. Some nitro and nitrosyl (NO^+) metal complexes have been shown to exist in a pH-dependent equilibrium,[12] and nitrosyl ligated to iron porphyrins is reduced to NH_3.[13] The mechanism concerning dissociation of NO from the reaction site, however, has hardly been discussed in reference to artificial NO_3^- and NO_2^- reductions. Recently, we reported assimilatory and dissimilatory reductions of NO_3^- by a $(Bu_4N)_3[Mo_2Fe_6S_8(SPh)_9]$-modified glassy-carbon electrode in H_2O[14] and dissimilatory reduction of NO_2^- by $[Fe_4S_4(SPh)_4]^{2-}$ in CH_3CN.[15] The active sites in these NO_n^- (n = 2, 3) reductions are provided by dissociation of PhS^- from Fe of the reduced forms of $[Mo_2Fe_6S_8(SPh)_9]^{3-}$ and $[Fe_4S_4(SPh)_4]^{2-}$. The reductions of NO_3^- and NO_2^- on an Mo atom, therefore, are of interest in connection with the active sites of molybdenum-containing nitrate reductases. For this purpose, a $(Bu_4N)_4[MoFe_3S_4(SPh)_3(O_2C_6Cl_4)]_2$-modified glassy-carbon electrode was used in the reduction of NO_3^- and NO_2^-, since various nucleophiles (L) selectively coordinate to the Mo atom of $[MoFe_3S_4(SR)_3(O_2C_6Cl_4)]_2^{4-}$ (R = alkyl and aryl) by breaking the Mo–(SR)Fe bond.[16] Part of this work has appeared recently.[17]

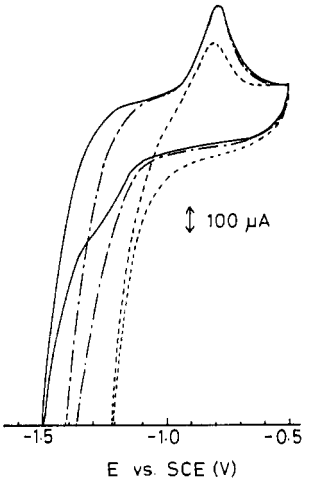

Figure 2. Cyclic voltammograms of the $(Bu_4N)_4[MoFe_3S_4(SPh)_3(O_2C_6Cl_4)]_2$ (50 nmol) modified glassy-carbon electrode ($[MoFe_3S_4]$/GC) in the absence (—) and presence of $NaNO_3$ (-·-) and $NaNO_2$ (---) (0.10 mol dm^{-3}) in H_2O (pH 10.0).

Experimental Section

Materials. Commercially available guaranteed reagent grade NaOH, H_3PO_4, $NaNO_2$, and $NaNO_3$ were used without further purification. Molybdenum–iron–sulfur clusters, $(Bu_4N)_4[MoFe_3S_4(SPh)_3(O_2C_6Cl_4)]_2$,[16] $(Bu_4N)_3[Mo_2Fe_6S_8(SPh)_9]$,[18] and $(Et_4N)_5[Mo_2Fe_6S_8(SPh)_9]$,[19] were prepared according to literature methods. Glassy-carbon plates with areas of 1.0 and 3.0 cm^2 (Tokai Carbon Co. Ltd., SC-2) were polished with Al_2O_3 (0.3 μm) and washed with distilled water several times. Electrical lead copper wires were attached with silver–epoxy resin to the back of the polished glassy-carbon plates, and then the back and round rims of the glassy-carbon plates were coated with epoxy resin. The $(Bu_4N)_4[MoFe_3S_4(SPh)_3(O_2C_6Cl_4)]_2$- and $(Bu_4N)_3[Mo_2Fe_6S_8(SPh)_9]$-modified glassy-carbon electrodes ($[MoFe_3S_4]$/GC and $[Mo_2Fe_6S_8]$/GC, respectively) were prepared by deposition of a given amount of a CH_3CN solution of each cluster (1.0×10^{-3} mol dm^{-3}) onto a polished surface of the glassy-carbon plates (1.0 and 3.0 cm^2) by syringe techniques and dried for ca. 30 min under dry N_2 stream.[14,20] The cluster-modified glassy-carbon electrodes thus prepared were used for the electrochemical measurements and the reduction of $NaNO_3$, $NaNO_2$, and N_2O in water (pH 10.0).

Physical Measurements. Electronic absorption spectra were measured with a Union SM-401 instrument, and FT-IR spectra were taken on Nicolet FT-IR 5DX and Shimadzu FTIR-8100 spectrophotometers. The equilibrium constant (K) for the reaction between $(Bu_4N)_2[MoFe_3S_4(SPh)_3(O_2C_6Cl_4)(DMF)]$ and $NaNO_2$ in DMF was obtained from the change of the absorbance at 450 nm of the CT band of the former in the presence of various amounts of the latter by using eq 1, where d_0, d, and

$$d = \frac{d_0 - d}{[NaNO_2]K} + d_\infty \qquad (1)$$

d_∞ are the absorbances of $[MoFe_3S_4(SPh)_3(O_2C_6Cl_4)(DMF)]^{2-}$, the equilibrium mixture of $[MoFe_3S_4(SPh)_3(O_2C_6Cl_4)(DMF)]^{2-}$ and $NaNO_2$, and their 1:1 adduct, respectively. Cyclic voltammograms were obtained by a use of a Hokuto Denko HB-401 potentiostat, a Hokuto Denko HB-107 function generator, and a Yokogawa Electric 3077 X-Y recorder. Voltammograms of rotating ring–disk electrodes (RRDE) were measured with a Hokuto Denko HR-101B dual potentiostat. Cathodic polarization of the $[MoFe_3S_4]$/GC (1.0 cm^2) in the absence and presence

(7) (a) Wharton, D. F. C.; Weintraub, S. T. *Biochem. Biophys. Res. Commun.* **1980**, *97*, 236. (b) Betlach, M. R.; Tiedje, J. M. *Appl. Environ. Microbiol.* **1981**, *42*, 1074. (c) Garber, E. A. E.; Hollocher, T. C. *J. Biol. Chem.* **1981**, *256*, 5459. (d) Yamanaka, T.; Ota, A.; Okunuki, K. *Biochim. Biophys. Acta* **1961**, *53*, 294. (e) Cox, C. D.; Payne, W. J. *Can. J. Microbiol.* **1973**, *19*, 861. (f) Matsubara, T.; Iwasaki, H. *J. Biochem. (Tokyo)* **1971**, *69*, 859. (g) Firestone, M. K.; Firestone, R. B.; Tiedje, J. M. *Biochem. Biophys. Res. Commun.* **1979**, *91*, 10. (h) Cox, C. D.; Payne, W. J.; DerVartanian, D. V. *Biochem. Biophys. Acta* **1971**, *253*, 290. (i) LeGall, J.; Payne, W. J.; Morgan, T. V.; DerVartanian, D. *Biochem. Biophys. Res. Commun.* **1979**, *87*, 355. (j) Johnson, M. K.; Thompson, A. J.; Walsh, T. A.; Barber, D.; Greenwood, C. *Biochem. J.* **1980**, *189*, 285.
(8) (a) Antonini, E.; Brunori, M. *Hemoglobin and Myoglobin in Their Reactions with Ligands*; North-Holland: Amsterdam, 1971; pp 161–231. (b) Yonetani, T.; Yamamoto, H.; Erman, J. E.; Leigh, J. S.; Reed, G. H. *J. Biol. Chem.* **1972**, *247*, 2447. (c) Henry, Y.; Mazza, G. *Biochim. Biophys. Acta* **1974**, *371*, 14.
(9) Chang, C. K. *J. Biol. Chem.* **1985**, *260*, 9520.
(10) (a) Pletcher, D.; Poorabedi, Z. *Electrochim. Acta* **1979**, *24*, 1253. (b) Moyer, B. A.; Meyer, T. J. *J. Am. Chem. Soc.* **1979**, *101*, 1326. (c) Horanyi, G.; Rizmayer, E. M. *J. Electroanal. Chem. Interfacial Electrochem.* **1985**, *180*, 265. (d) Taniguchi, I.; Nakashima, N.; Yasukouchi, K. *J. Chem. Soc., Chem. Commun.* **1986**, 1814. (e) Li, H. L.; Robertson, D. H.; Chambers, J. Q.; Hobbs, D. T. *J. Electrochem. Soc.* **1988**, *35*, 1154.
(11) (a) Frank, A. J.; Gratzel, M. *Inorg. Chem.* **1982**, *21*, 3834. (b) Halmann, M.; Tobin, J.; Zuckerman, K. *J. Electroanal. Chem. Interfacial Electrochem.* **1986**, *209*, 405. (c) Kudo, A.; Domen, K.; Maruya, K.; Onishi, T. *Chem. Lett.* **1987**, 1019. (d) Willner, I.; Lapidot, N.; Riklin, A. *J. Am. Chem. Soc.* **1989**, *111*, 1883.
(12) Murphy, W. R.; Takeuchi, K.; Barley, M. H.; Meyer, T. J. *Inorg. Chem.* **1986**, *25*, 1041.
(13) Barley, M. H.; Takeuchi, K. J.; Meyer, T. J. *J. Am. Chem. Soc.* **1986**, *108*, 5876.
(14) Kuwabata, S.; Uezumi, S.; Tanaka, K.; Tanaka, T. *Inorg. Chem.* **1986**, *25*, 3018.
(15) Tanaka, K.; Wakita, R.; Tanaka, T. *J. Am. Chem. Soc.* **1989**, *111*, 2428.
(16) (a) Armstrong, W. H.; Maschark, P. K.; Holm, R. H. *J. Am. Chem. Soc.* **1982**, *104*, 4373. (b) Maschark, P. K.; Armstrong, W. H.; Mizobe, Y.; Holm, R. H. *J. Am. Chem. Soc.* **1983**, *105*, 475. (c) Palermo, R. E.; Singh, R.; Bashkin, J. K.; Holm, R. H. *J. Am. Chem. Soc.* **1984**, *106*, 2600.
(17) Tanaka, K.; Matsui, T.; Tanaka, T. *Chem. Lett.* **1989**, 1827.
(18) Christou, G.; Garner, C. D. *J. Chem. Soc., Dalton Trans.* **1980**, 2354.
(19) Christou, G.; Mascharak, P. K.; Armstrong, W. H.; Papaefthymiou, G. C.; Frankel, R. B.; Holm, R. H. *J. Am. Chem. Soc.* **1982**, *104*, 2820.
(20) Tanaka, K.; Uezumi, S.; Tanaka, T. *J. Chem. Soc., Dalton Trans.* **1989**, 1547.

of NO_2^- was conducted without stirring the aqueous phase. The current–potential curves of the $[MoFe_3S_4]$/GC were obtained after reaching a constant cathodic current intensity at each applied potential.

Reductions of NO_3^- and NO_2^- by the Cluster-Modified Glassy-Carbon Electrodes. The reductions of $NaNO_3$ and $NaNO_2$ were carried out under controlled-potential electrolysis conditions in an aqueous buffer solution (pH 10.0, $NaOH-H_3PO_4$, 0.5 mol dm^{-3}) at 298 K under He atmosphere with the use of an electrolysis cell consisting of three compartments: one for the cluster-modified glassy-carbon electrode (3.0 cm^2), the second for a platinum counter electrode (3.0 cm^2), which was separated from the cluster-modified glassy-carbon electrode by a cation-exchange membrane (Nafion film), and the third for an SCE reference electrode. The number of coulombs consumed in the reduction was measured with a Hokuto Denko HF-201 coulometer. Gas analysis was performed on a Shimadzu GC-3BT gas chromatograph packed with 13X molecular sieves. Ammonia was analyzed with a Shimadzu GC-6A gas chromatograph packed with Chromosorb 103. The concentration of NO_2^- in the aqueous solution was determined by colorimetric titration.[21] The details of the analytical conditions were described in a previous paper.[14]

Results and Discussion

Redox Behavior of the $(Bu_4N)_4[MoFe_3S_4(SPh)_3(O_2C_6Cl_4)]_2$-Modified Glassy-Carbon Electrode in Water. The redox behavior of the $(Bu_4N)_4[MoFe_3S_4(SPh)_3(O_2C_6Cl_4)]_2$-modified glassy-carbon plate ($[MoFe_3S_4]$/GC)[20] was examined in the absence and presence of NO_3^- and NO_2^- in H_2O (pH 10.0) in order to elucidate the ability of the $[MoFe_3S_4]$/GC to catalyze the reduction of these substrates. The cyclic voltammogram of the $[MoFe_3S_4]$/GC shows an anodic wave at −0.79 V vs SCE and a cathodic one around −1.30 V, followed by a strong cathodic current due to H_2 evolution catalyzed by the reduced species of the cluster,[22] as shown by the solid curve in Figure 2. The pattern of the cathodic wave of the $[MoFe_3S_4]$/GC is somewhat ambiguous, although the number of coulombs calculated from the area of the −0.79-V anodic wave is consistent with two electrons per molecule of $(Bu_4N)_4[MoFe_3S_4(SPh)_3(O_2C_6Cl_4)]_2$ modified ($n = 2.00 \pm 0.06$). Thus, all the clusters modified on the GC plate participate in the redox reaction even in the solid state. The cyclic voltammograms of the $[MoFe_3S_4]$/GC in the presence of $NaNO_2$ and $NaNO_3$ show an increase in the cathodic currents at potentials more negative than −1.20 V compared with the absence of them, and the cathodic wave of the $[MoFe_3S_4]$/GC is completely concealed. Neither NO_2^- nor NO_3^- is reduced by the GC plate at potentials more positive than −1.70 V in H_2O (pH 10.0). Thus, the $[MoFe_3S_4]$/GC has the ability to catalyze the reduction of both NO_3^- and NO_2^-. The onset potential of the reduction of NO_3^- is essentially consistent with that of the cathodic wave of $[MoFe_3S_4]$/GC, while the reduction of NO_2^- takes place about 200 mV more positive than the onset potential of the reduction of NO_3^-, suggesting that NO_2^- is much more subject to reduction than NO_3^- and H^+ by the $[MoFe_3S_4]$/GC. The decrease in the −0.79-V anodic wave of the $[MoFe_3S_4]$/GC is largely dependent on the concentration of NO_2^- in the aqueous phase, since the wave almost disappeared in the presence of more than 0.20 mol dm^{-3} $NaNO_2$. Even under such conditions, the solid cyclic voltammogram of Figure 2 was regenerated after replacement of the aqueous $NaNO_2$ solution by $NaNO_2$-free H_2O (pH 10.0). This result indicates that most of the electrons transferred to the cluster in the cathodic scan are consumed in the reduction of NO_2^- prior to the anodic process of the cluster in the anodic scan. Thus, the pattern of the cyclic voltammogram of the $[MoFe_3S_4]$/GC is largely influenced by the rate of the chemical reactions catalyzed by the cluster.

The stability of the $[MoFe_3S_4]$/GC was dependent on the experimental conditions; the peak current of the −0.79-V anodic wave of the $[MoFe_3S_4]$/GC decreased to 80% of its original value in the multiscanning cyclic voltammogram in H_2O (pH 10.0) for 1 h, while the cyclic voltammogram of the $[MoFe_3S_4]$/GC was essentially unchanged even after the controlled-potential electrolysis at −1.25 V in a stirred aqueous solution (pH 10.0) for 4 h.[23] It is worthy of note that the redox reaction of the modified electrode is accompanied by the transport of the counterion into and out of the contacting electrolyte solution to maintain charge neutrality. Accordingly, the multiscanning cyclic voltammogram causes a constant movement of the counterion on the $[MoFe_3S_4]$/GC, which accelerates more or less the detachment of the cluster from the GC plate. The enhancement in the stability of the $[MoFe_3S_4]$/GC under controlled-potential electrolysis conditions, therefore, may result from the decrease in the movement of the counterion on the modified electrode. Furthermore, the cyclic voltammogram of the MoFeS cluster extracted with a DMF solution of Bu_4NBr (5 cm^3, 0.10 mol dm^{-3}) from the $[MoFe_3S_4]$/GC (2.75×10^{-6} mol) after the controlled-potential electrolysis at −1.00 V vs SCE in an aqueous $NaNO_2$ (0.05 mol dm^{-3}) solution for 3 h was almost completely consistent with that of $(Bu_4N)_4[MoFe_3S_4(SPh)_3(O_2C_6Cl_4)]_2$ ($E_{pc} = -1.12$ and $E_{pa} = -1.03$ V vs SCE) in the same solvent (1.9 mmol dm^{-3}). This result indicates that the solid state of $(Bu_4N)_4[MoFe_3S_4(SPh)_3(O_2C_6Cl_4)]_2$ on the GC plate hardly undergoes a hydrolysis reaction during the electrolysis in H_2O (pH 10.0). The large cathodic current due to the reduction of NO_2^- also decreases the stability of the $[MoFe_3S_4]$/GC; the cyclic voltammogram of the $[MoFe_3S_4]$/GC in H_2O (pH 10)[24] after the controlled-potential electrolysis of the $[MoFe_3S_4]$/GC in a stirred aqueous $NaNO_2$ solution (0.10 mol dm^{-3}) at −1.25 V for 4 h and at −1.00 V for 48 h showed 50 and 75% decrease in the −0.79-V anodic peak currents compared with the initial values in H_2O. It is, however, worthy of note that the amount of the cluster required to catalyze the reductions of NO_3^- and NO_2^- may be sufficient at concentrations as low as 10^{-9}–10^{-10} mol cm^{-2} on the GC plate (monomolecular layer), since the reductions take place at the surface of the $[MoFe_3S_4]$/GC. In fact, a $(Bu_4N)_3[Mo_2Fe_6S_8(SPh)_9]$-modified GC electrode ($[Mo_2Fe_6S_8]$/GC) exhibits the highest activity at a surface concentration of (1.4–2.2) $\times 10^{-9}$ mol cm^{-2} toward the reduction of organic azide in H_2O.[25] The slow decrease in the amount of $(Bu_4N)_4[MoFe_3S_4(SPh)_3(O_2C_6Cl_4)]_2$ modified on the GC plate during the electrolysis, therefore, is not considered to have a serious effect on the rate of the reductions of NO_3^- and NO_2^-, unless the amount of the cluster on the GC plate becomes less than 10^{-9} mol cm^{-2}.

Cathodic polarization of the $[MoFe_3S_4]$/GC was conducted in the absence and presence of NO_2^- to obtain more information about the NO_2^- reduction. The increase in the cathodic current

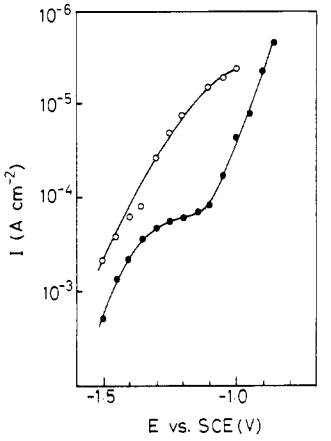

Figure 3. Cathodic polarizations of the $[MoFe_3S_4]$/GC (50 nmol) in the absence (○) and presence of $NaNO_2$ (●) (0.10 mol dm^{-3}) in H_2O (pH 10.0).

(21) Shinn, M. B. *Ind. Eng. Chem., Anal. Ed.* **1941**, *13*, 33.
(22) H_2 evolution on the GC plate did not take place up to −1.70 V at pH 10.0.
(23) The cyclic voltammogram of the $[MoFe_3S_4]$/GC after the controlled-potential electrolysis at −1.00 V in a stirred aqueous phase (pH 10.0) for 48 h showed a 20% decrease in the peak current of the −0.79-V anodic wave compared with its initial value.
(24) The cyclic voltammogram of the $[MoFe_3S_4]$/GC used in the reduction of $NaNO_2$ was obtained after the electrode had been washed with O_2-free water several times.
(25) Kuwabata, S.; Tanaka, K.; Tanaka, T. *Inorg. Chem.* **1986**, *25*, 1691.

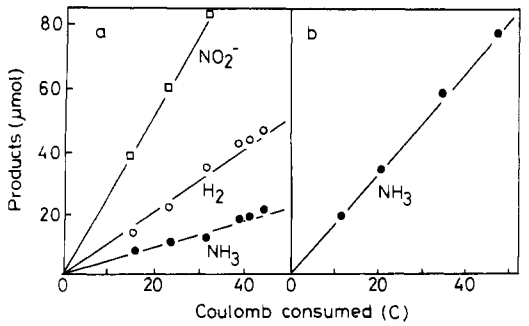

Figure 4. Reduction of NO_n^- (n = 2, 3) by the $[MoFe_3S_4]$/GC (50 nmol) under controlled-potential electrolysis at −1.25 V vs SCE in aqueous $NaNO_3$ (a) and $NaNO_2$ (b) solutions (50 mmol dm^{-3}) at pH 10.0.

Table I. Reduction of $NaNO_3$, $NaNO_2$, and N_2O by the $(Bu_4N)_4[MoFe_3S_4(SPh)_3(O_2C_6Cl_4)]_2$ (50 nmol) Modified Glassy-Carbon Electrode in H_2O (pH 10.0)

				amt of products/μmol			
entry	substrate	E/V	time/h	NH_3	N_2	NO_2^-	H_2
1	NO_3^-[a]	−1.25	4.5	21	0	96	46
2	NO_2^-[b]	−1.25	4.5	42	0		30
3	NO_2^-[a]	−1.25	4.5	100	0		7
4	NO_2^-[a]	−1.00	48	10	180		0
5	N_2O[c]	−1.00	48	0	160		0

[a] 700 μmol. [b] 70 μmol. [c] Saturated in H_2O.

of the $[MoFe_3S_4]$/GC at potentials more negative than −1.0 V results from H_2 evolution in H_2O (○ in Figure 3). As expected from the cyclic voltammogram of Figure 2, the I–E curve of the $[MoFe_3S_4]$/GC in the presence of $NaNO_2$ is shifted to positive potentials compared with that in H_2O; the current intensity increases up to −1.1 V and then levels off in the potential region of −1.1 to −1.3 V (● in Figure 3) due to the limiting current of the reduction of NO_2^- (vide infra). The further increase in the cathodic current at potentials more negative than −1.3 V may be caused by combination of the reduction of NO_2^- and H_2 evolution.

Reductions of NO_3^- and NO_2^- by the $[MoFe_3S_4]$/GC Electrode. The controlled-potential electrolysis of the $[MoFe_3S_4]$/GC (50 nmol) at −1.25 V vs SCE in an aqueous $NaNO_3$ (50 mmol dm^{-3}) solution (pH 10.0) produces NO_2^-, NH_3, and H_2, as depicted in Figure 4a. On the basis of the stoichiometries of eqs 2–4, the

$$NO_3^- + 2H^+ + 2e^- \rightarrow NO_2^- + H_2O \quad (2)$$

$$NO_3^- + 9H^+ + 8e^- \rightarrow NH_3 + 3H_2O \quad (3)$$

$$2H^+ + 2e^- \rightarrow H_2 \quad (4)$$

current efficiencies for the formation of NO_2^-, NH_3, and H_2 were 42, 37, and 20%, respectively, in 4.5 h (Table I). Thus, no other reaction took place under the experimental conditions. Gradual accumulation of free NO_2^- in the aqueous phase suggests that NO_3^- is first reduced to NO_2^- (eq 2), which then undergoes further six-electron reduction to afford NH_3 (eq 5). In accordance with

$$NO_2^- + 7H^+ + 6e^- \rightarrow NH_3 + 2H_2O \quad (5)$$

this, the reduction of $NaNO_2$ in H_2O (50 mmol dm^{-3}) using the same electrode selectively produced NH_3 with a current efficiency 96% (Figure 4b and entry 3 in Table I). Such a large difference in the current efficiency for the formation of NH_3 in the reductions of NO_3^- (eq 3) and NO_2^- (eq 5) can be associated with the current densities at −1.25 V in the cyclic voltammograms of the $[MoFe_3S_4]$/GC in aqueous $NaNO_3$ and $NaNO_2$ solutions (Figure 2). The limiting current observed in the potential region of −1.1 to −1.3 V in the cathodic polarization of the $[MoFe_3S_4]$/GC (● in Figure 3), therefore, may result from the selective assimilatory reduction of NO_2^-.

The reduction of NO_2^- by the $[MoFe_3S_4]$/GC under the electrolysis at −1.00 V vs SCE produced not only N_2 (eq 6) but

$$2NO_2^- + 8H^+ + 6e^- \rightarrow N_2 + 4H_2O \quad (6)$$

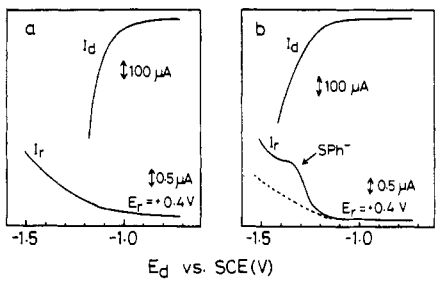

Figure 5. I_d and I_r curves at E_r = +0.40 V of the RRDE having $[MoFe_3S_4]$/GC (a) and $[Mo_2Fe_6S_8]$/GC disk electrodes (b) (56 nmol) in aqueous $NaNO_2$ (0.10 mol dm^{-3}). dE/dt = 10 mV s^{-1} and ω = 1000 rpm.

also NH_3 (eq 5) with current efficiencies 90 and 6%, respectively (entry 4 in Table I). Thus, a positive shift of the $[MoFe_3S_4]$/GC potential brings about the preferential dissimilatory reduction of NO_2^- (eq 6). Although we could not detect N_2O in the reduction of NO_2^- by the $[MoFe_3S_4]$/GC at −1.00 V, the controlled-potential electrolysis of the $[MoFe_3S_4]$/GC at −1.00 V in an N_2O-saturated aqueous solution (pH 10) produced N_2 with a current efficiency of almost 100% (entry 5 in Table I), suggesting that N_2O is the precursor of N_2 in the present dissimilatory reduction of NO_2^-.

Intermediate in the Reduction of NO_2^-. A positive shift of the $[MoFe_3S_4]$/GC potential from −1.25 to −1.00 V in the reduction of NO_2^- caused an alternation in the main product from NH_3 to N_2. A similar observation has been reported in an electrochemical NO_2^- reduction catalyzed by iron porphyrin[13] and $(Bu_4N)_3[Mo_2Fe_6S_8(SPh)_9]$.[14] This may be indicative of the presence of a common intermediate in both reduction paths. A rotating ring–disk electrode (RRDE) comprising the $[MoFe_3S_4]$/GC disk and a glassy-carbon ring electrode was used in the reduction of NO_2^- in order to detect the intermediate involved in the six-electron jump from NO_2^- to NH_3 (eq 5) or four-electron jump to N_2O. The current–potential (I_d–E_d) curve of the rotating $[MoFe_3S_4]$/GC disk electrode (ω = 1000 rpm) in aqueous $NaNO_2$ solution (pH 10.0) shows that the reduction of NO_2^- by the $[MoFe_3S_4]$/GC disk electrode takes place at potentials more negative than E_d = −0.90 V vs SCE (upper curve in Figure 5a). At the same time, an anodic current (I_r) begins to flow at the ring electrode fixed at E_r = +0.40 V vs SCE and increases with increasing cathodic current I_d (lower line in Figure 5a). The glassy-carbon ring electrode can oxidize neither NO_2^-, NH_3, N_2O, nor H_2 at +0.40 V vs SCE in H_2O (pH 10.0). The increase in I_r, therefore, is reasonably assigned to the oxidation process of the reaction intermediate involved in the reduction of NO_2^- by the $[MoFe_3S_4]$/GC disk electrode.

For comparison of the catalytic abilities of $(Bu_4N)_4[MoFe_3S_4(SPh)_3(O_2C_6Cl_4)]_2$ and $(Bu_4N)_3[Mo_2Fe_6S_8(SPh)_9]$ in the reduction of NO_2^-, the I_d–E_d and I_r–E_d curves (at E_r = +0.4 V) of the RRDE (ω = 1000 rpm) having $(Bu_4N)_3[Mo_2Fe_6S_8(SPh)_9]$-modified glassy-carbon disk ($[Mo_2Fe_6S_8]$/GC)[14] and glassy-carbon ring electrodes (at E_r = +0.40 V) are also illustrated in Figure 5b. The onset potential of the reduction of NO_2^- (50 mmol dm^{-3}) by the $[Mo_2Fe_6S_8]$/GC disk electrode is about 200 mV more negative than that of the reduction by the $[MoFe_3S_4]$/GC (compare the I_d–E_d curves of Figure 5b and Figure 5a). The reduction of NO_2^- by the reduced species $[Mo_2Fe_6S_8(SPh)_9]^{3-}$[14] and $[Fe_4S_4(SPh)_4]^{2-}$[15] takes place on the Fe atoms with dissociating PhS^- ligated, and NH_2OH is identified as the reaction intermediate in the reduction catalyzed by $[Mo_2Fe_6S_8(SPh)_9]^{3-}$. In accordance with this, the ring electrode detects the oxidation process of PhS^- liberated from the $[Mo_2Fe_6S_8]$/GC disk electrode[25,26] as a shoulder around E_d = −1.3

(26) On the basis of a collection coefficient value of the RRDE obtained by the redox couple of Fe^{2+}/Fe^{3+} in H_2O, the amount of PhS^- dissociated from the $[Mo_2Fe_6S_8]$/GC was determined as 2.5 mol/mol of the cluster. However, such a collection coefficient determined in a homogeneous solution cannot be used for the RRDE having the $[Mo_2Fe_6S_8]$/GC disk electrode, since the dissociation of PhS^- is caused by the bond fission from the surface of the disk electrode.

Scheme I

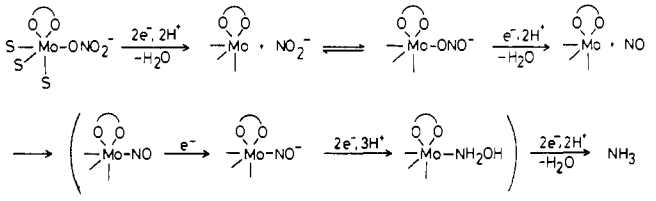

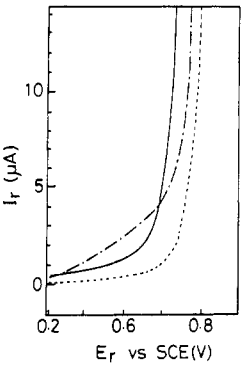

Figure 6. E_r–I_r curves of the RRDE having the $[MoFe_3S_4]$/GC disk electrode (E_d = −0.60 (---) and −1.50 V (—)) and the $[Mo_2Fe_6S_8]$/GC disk electrode (E_d = −1.50 V (-·-)) in an aqueous $NaNO_2$ solution (0.10 mol dm^{-3}). dE/dt = 10 mV s^{-1} and ω = 1000 rpm.

V. After a few potential sweeps of the $[Mo_2Fe_6S_8]$/GC disk electrode, the anodic ring current due to the oxidation of PhS^- disappears in the I_r–E_d curve at E_r = +0.40 V, and only the anodic current resulting from the oxidation of NH_2OH formed on the $[Mo_2Fe_6S_8]$/GC disk electrode is observed on the ring electrode[14] (dotted line in Figure 5b). The observation that the oxidation current of PhS^- is not clearly detected in the I_r–E_d curve of the RRDE having the $[MoFe_3S_4]$/GC disk electrode (Figure 5a) suggests that dissociation of PhS^- from the Fe atoms of the $MoFe_3S_4$ core can almost be neglected in the initial stage of the reduction of NO_2^- by the $[MoFe_3S_4]$/GC. This is consistent with the fact that the Mo atom of $[MoFe_3S_4(SR)_3(O_2C_6Cl_4)]_2^{4-}$ is much more subject to a nucleophilic reaction than the Fe atoms of the $MoFe_3S_4$ core, since two Mo–(SR)Fe bridging moieties of $[MoFe_3S_4(SR)_3(O_2C_6Cl_4)]_2^{4-}$ (R = alkyl and aryl) are selectively cleaved in polar solvents by coordination of the solvent molecule to the Mo atom, generating two single cubane clusters $[MoFe_3S_4(SR)_3(O_2C_6Cl_4)(L)]^{2-}$ (L = solvents) (eq 7), and the

$$[MoFe_3S_4(SR)_3(O_2C_6Cl_4)]_2^{4-} + 2L \rightarrow 2[MoFe_3S_4(SR)_3(O_2C_6Cl_4)(L)]^{2-} \quad (7)$$

L = DMF, CH_3CN, THF, $CH_3C(O)CH_3$

solvated molecules are selectively substituted by various nucleophiles such as PR_3, RS^-, N_3^-, and NH_2NH_2.[16] The reduction of NO_n^- (n = 2, 3) by the $[MoFe_3S_4]$/GC, therefore, is considered to take place mainly on the Mo atom rather than on the Fe atoms.

Scheme II

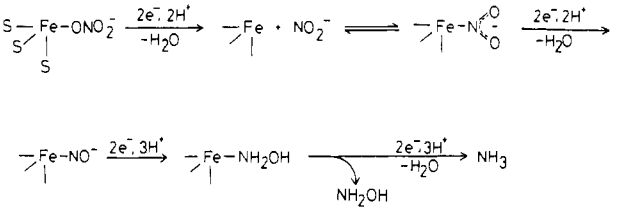

Figure 6 shows the I_r–E_r curves of the RRDE having the $[MoFe_3S_4]$/GC disk electrode at E_d = −0.60 (---) and −1.50 V (—) together with that of the RRDE having the $[Mo_2Fe_6S_8]$/GC disk electrode (-·-) in the presence of $NaNO_2$ (0.10 mol dm^{-3}) in H_2O (pH 10.0). The I_r–E_r curve at E_d = −0.60 V (dotted line in Figure 6) is consistent with the anodic current of the oxidation of NO_2^- (eq 8) on the glassy-carbon ring electrode, since no

$$NO_2^- + H_2O \rightarrow NO_3^- + 2H^+ + 2e^- \quad (8)$$

electrochemical reaction takes place on the $[MoFe_3S_4]$/GC disk electrode at −0.60 V (see the I_d–E_d curves in Figure 5). The I_r–E_r curve at E_d = −1.50 V of the $[Mo_2Fe_6S_8]$/GC disk electrode (-·-) has been assigned to the oxidation of NH_2OH (eq 9) generated

$$NO_2^- + 5H^+ + 4e^- \rightarrow NH_2OH + H_2O \quad (9)$$

by four-electron reduction of NO_2^- by the $[Mo_2Fe_6S_8]$/GC disk electrode.[14] It should be noticed that the I_r–E_r curves of the $[MoFe_3S_4]$/GC (—) and the $[Mo_2Fe_6S_8]$/GC disk electrodes (-·-) at E_d = −1.50 V intersect with each other. This result indicates that the intermediate in the reduction of NO_2^- by the $[MoFe_3S_4]$/GC is different from NH_2OH. Although NO_2^- is stable under electrolysis at −1.25 V by the GC electrode in H_2O (pH 10.0), it can be reduced at a moderate rate at potentials more negative than −2.0 V with concomitant violent H_2 evolution. As H_2 is not oxidized by the GC plate, the initial product in the reduction of NO_2^- by the GC disk plate, therefore, may be detected by using an RRDE. When NO_2^- (0.10 mol dm^{-3}) was reduced on the GC disk electrode (not modified with $(Bu_4N)_4$-$[MoFe_3S_4(SPh)_3(O_2C_6Cl_4)]_2$) of the RRDE ($\omega$ = 1000 rpm) at −2.20 V in H_2O (pH 10.0), the ring electrode showed the same I_r–E_r curve as that of the solid line of Figure 6. In addition, the solid I_r–E_r curve of Figure 6 was also obtained in an anodic sweep of E_r (without applying potentials to the GC disk electrode) of the RRDE (ω = 1000 rpm) by bubbling NO into an aqueous $NaNO_2$ solution (0.10 mol dm^{-3}) at pH 10.0.[27] The most possible

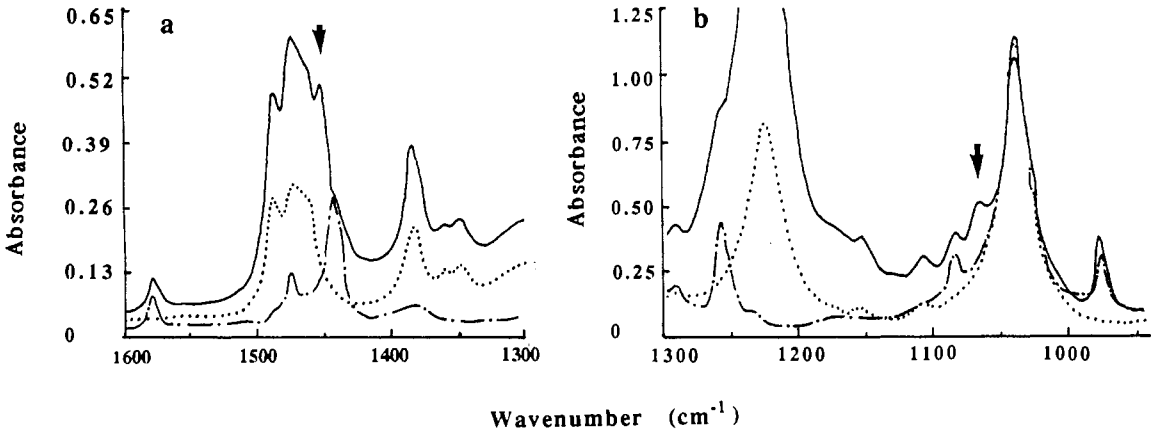

Figure 7. FT-IR spectra of $(Bu_4N)_2[MoFe_3S_4(SPh)_3(O_2C_6Cl_4)(CD_3CN)]$ (0.02 mol dm^{-3}) (-·-), Bu_4NNO_2 (0.27 mol dm^{-3}) ···), and their mixture (0.02 and 0.54 mol dm^{-3}, respectively) (—) in CD_3CN (a) and those of $(Bu_4N)_2[MoFe_3S_4(SPh)_3(O_2C_6Cl_4)(CH_3CN)]$ (0.04 mol dm^{-3}) (-·-), Bu_4NNO_2 (0.31 mol dm^{-3}) (···), and their mixture (0.04 and 0.90 mol dm^{-3}) (—) in CH_3CN (b).

reaction intermediate in the reduction of NO_2^- by the $[MoFe_3S_4]$/GC, therefore, may be assigned to NO formed by one-electron reduction (eq 10) on the $[MoFe_3S_4]$/GC. It is well-known that NO_2^- exists as an equilibrium mixture with HNO_2 ($pK_a = 4.06$[28]) under acidic conditions and decomposes to NO and HNO_3 by a disproportionation reaction (eqs 11 and 12).[29]

$$NO_2^- + 2H^+ + e^- \rightarrow NO + H_2O \quad (10)$$

$$NO_2^- + H^+ \rightleftharpoons HNO_2 \quad (11)$$

$$3HNO_2 \rightarrow HNO_3 + 2NO + H_2O \quad (12)$$

Accordingly, the reduction of NO_2^- conducted under strongly acidic conditions is accompanied by concomitant NO evolution.[13] The $pK_a = 4.06$ of HNO_2, however, may reasonably exclude the possibility of the reactions 11 and 12 in the present NO_2^- reduction at pH 10.0.

Interaction between $(Bu_4N)_4[MoFe_3S_4(SPh)_3(O_2C_6Cl_4)]_2$ and NO_2^- in Solution. The electrochemical study indicates that not only the binding sites but also the intermediate involved in the reduction of NO_2^- by the $[MoFe_3S_4]$/GC and $[Mo_2Fe_6S_8]$/GC are different from each other. Although $(Bu_4N)_4[MoFe_3S_4(SPh)_3(O_2C_6Cl_4)]_2$ exists in the solid state in the $[MoFe_3S_4]$/GC, the interaction between NO_2^- and the cluster was examined in DMF. The CT band of $[MoFe_3S_4(SPh)_3(O_2C_6Cl_4)(DMF)]^{2-}$ at 450 nm in the electronic absorption spectrum recorded in DMF gradually decreased with the appearance of an isosbestic point at 325 nm resulting from the addition of $NaNO_2$ to the solution. Such a spectral change may be explained by NO_2^- substitution of the DMF ligand on Mo in $[MoFe_3S_4(SPh)_3(O_2C_6Cl_4)(DMF)]^{2-}$ (eq 13), similar to substitutions of solvated molecules by various nucleophiles.[16] The equilibrium constant (eq 13) calculated from the change of the absorbance at 450 nm was 30 ± 2 mol^{-1} dm^3 at 298 K (see Experimental Section).

$$[MoFe_3S_4(SPh)_3(O_2C_6Cl_4)(DMF)]^{2-} + NO_2^- \rightleftharpoons [MoFe_3S_4(SPh)_3(O_2C_6Cl_4)(NO_2)]^{3-} + DMF \quad (13)$$

It is well-known that NO_2^- coordinates to a metal in a variety of forms such as nitro, nitrito, chelating nitro, and bridging nitro.[30] Taking into account the coordination number of Mo in the $MoFe_3S_4$ core, NO_2^- may bind to the Mo with either nitrogen (Mo–NO_2^-) or oxygen (Mo–ONO^-) in a monodentate form. Nitro (Mo–NO_2^-) and nitrito (Mo–ONO^-) adducts can be distinguished from the stretching frequencies of the coordinated NO_2^-; for nitro complexes, typical $\nu_a(NO_2)$ and $\nu_s(NO_2)$ values are 1470–1370 and 1340–1320 cm^{-1}, respectively, and for nitrito complexes, ν(N=O) and ν(NO) are in the ranges 1485–1400 and 1110–1050 cm^{-1}.[30] The FT-IR spectrum of a CD_3CN solution[31] containing $(Bu_4N)_2[MoFe_3S_4(SPh)_3(O_2C_6Cl_4)(CD_3CN)]$ (20 mmol dm^{-3}) and Bu_4NNO_2 (0.54 mol dm^{-3}) exhibited six bands between 1500 and 1300 cm^{-1}. Five bands of those waves are assigned to either $(Bu_4N)_2[MoFe_3S_4(SPh)_3(O_2C_6Cl_4)(CD_3CN)]$ or Bu_4NNO_2 on the basis of the agreement of the wavenumbers of each compound (Figure 7a). The remaining 1453-cm^{-1} band, therefore, may be assigned to the adduct. In addition, the CH_3CN solution of $(Bu_4N)_2[MoFe_3S_4(SPh)_3(O_2C_6Cl_4)(CH_3CN)]$ (40 mmol dm^{-3}) and Bu_4NNO_2 (0.90 mol dm^{-3}) showed a new band at 1065 cm^{-1} as a shoulder of the solvent peak (Figure 7b). This observation suggests that the 1453- and 1065-cm^{-1} bands may be assigned to ν(N=O) and ν(NO) of the nitrito adduct formed in the reaction of $[MoFe_3S_4(SPh)_3(O_2C_6Cl_4)(L)]^{2-}$ (L = CH_3CN, CD_3CN) with NO_2^-. On the other hand, the CH_3CN solution containing Bu_4NNO_2 (0.20 mol dm^{-3}) and $(Et_4N)_5[Mo_2Fe_6S_8(SPh)_9]$ (40 mmol dm^{-3}) did not show any assignable ν(NO) band in the region 1110–1050 cm^{-1}, and the same mixture in CD_3CN displayed new bands at 1430 and 1323 cm^{-1}, assignable to $\nu_a(NO_2)$ and $\nu_s(NO_2)$. Therefore, NO_2^- is considered to bind to an Fe atom of $[Mo_2Fe_6S_8(SPh)_9]^{5-}$ with the nitrogen atom (nitro form), as suggested elsewhere.[15]

Possible Pathways of the Reductions of NO_3^- and NO_2^-. Neither NO_3^- nor NO_2^- is reduced at all by the GC electrode under electrolysis at −1.25 V in H_2O (pH 10.0). The reductions of NO_3^- and NO_2^-, therefore, are catalyzed by the $[MoFe_3S_4]$/GC. From a consideration of the interaction of $[MoFe_3S_4(SPh)_3(O_2C_6Cl_4)(L)]^{2-}$ (L = CH_3CN, CD_3CN) with NO_2^-, it is reasonably assumed that not only NO_2^- but also NO_3^- preferentially bind to Mo rather than to the Fe atoms of the $[MoFe_3S_4]$/GC via an oxygen atom. The reductions of NO_3^- and NO_2^-, therefore, are considered to take place mainly on the Mo atom of the $[MoFe_3S_4]$/GC. Despite the fact that NO_2^- is much more subject to reduction by the $[MoFe_3S_4]$/GC than NO_3^-, the former is gradually accumulated in the aqueous phase in the progress of the reduction of NO_3^- by the $[MoFe_3S_4]$/GC at −1.25 V (Figure 4a). It, therefore, is assumed that the dissociation of NO_2^- from the $[MoFe_3S_4]$/GC is caused by removal of the bound oxygen of the Mo–ONO_2^- moiety in the reduction of NO_3^- (Scheme I). As described in a previous section, free NO is the most possible intermediate in the following NO_2^- reduction. Similarly, the removal of the bound oxygen from the Mo–ONO^- moiety on the $[MoFe_3S_4]$/GC may also lead to dissociation of NO. Alternatively, even if the terminal oxygen of the Mo–ONO^- moiety is removed in the reduction, dissociation of NO is expected from the instability of the resulting oxygen-bound nitrosyl complex (Mo–ON). Recombination of NO with the $[MoFe_3S_4]$/GC is considered to be a very fast process, since the RRDE hardly detected the I_r–E_r curve of the reaction intermediate at slower rotation (ω < 500 rpm). A nitrosyl adduct thus formed may, therefore, be reduced to NH_3 possibly via NO^- and NH_2OH under electrolysis at −1.25 V (Scheme I). On the other hand, NO_2^- presumably binds to the Fe atom of the $[Mo_2Fe_6S_8]$/GC[14] via the nitrogen atom (a nitro form). The absence of a free NO intermediate in the reduction of NO_2^- by the $[Mo_2Fe_6S_8]$/GC may be explained by the assumption that the removal of oxygen from the Fe–NO_2^- moiety on the $[Mo_2Fe_6S_8]$/GC is not accompanied by bond fission between iron and nitrogen, and the resulting Fe–NO (or Fe–NO^-) moiety is further reduced to NH_3 via NH_2OH (Scheme II).

The reduction of NO_2^- by $[Fe_4S_4(SPh)_4]^{2-}$ effectively produces N_2 via NO^-, $N_2O_2^{2-}$, and N_2O under electrolysis at −1.25 V in CH_3CN.[15] Similarly, NO_2^- is reduced to N_2O via NO^- and $N_2O_2^{2-}$ in an oxo abstraction by $MoO(S_2CNEt_2)_2$ in DMF.[32] On the basis of the fast recombination of the possible intermediate NO with the $[MoFe_3S_4]$/GC, a nitrosyl adduct also may be involved in the present dissimilatory reduction of NO_2^- by the $[MoFe_3S_4]$/GC. One-electron reduction of the nitrosyl intermediate may cause the dissociation of NO^- from the $[MoFe_3S_4]$/GC to form $N_2O_2^{2-}$ in H_2O. Although we could not obtain direct evidence for the formation of $N_2O_2^{2-}$ in the reduction of NO_2^- at −1.00 V, this may be partly due to the decomposition to N_2O in H_2O. The present study indicates that the difference in the intermediate in the reductions of NO_2^- by the $[MoFe_3S_4]$/GC and $[Mo_2Fe_6S_8]$/GC is explained by the patterns of coordination of NO_2^- to the active sites of those electrodes. In addition, the $[MoFe_3S_4]$/GC shows a higher activity than the $[Mo_2Fe_6S_8]$/GC toward the reduction of NO_2^-; the former can reduce NO_2^- to N_2 under electrolysis at −1.00 V, while the latter has no ability to reduce N_2O even at −1.10 V. Therefore, NO_2^- is reduced up to N_2O by the latter under electrolysis at −1.10 V.[33]

(27) A clear limiting current of either the anodic or the cathodic process for pure NO was not detected by the use of the RRDE at pH 10.
(28) Gratzel, M.; Taniguchi, S.; Henglein, A. *Ber. Bunsen-Ges. Phys. Chem.* **1970**, *74*, 1003.
(29) (a) Cotton, F. A.; Wilkinson, G. *Advanced Inorganic Chemistry*, 4th ed.; Wiley: New York, 1980; p 430. (b) Stedman, G. *Adv. Inorg. Chem. Radiochem.* **1979**, *22*, 113.
(30) Nakamoto, K. *Infrared and Raman Spectra of Inorganic and Coordination Compounds*, 3rd ed.; Wiley-Interscience: New York, 1977; pp 220–225.
(31) DMF and CH_3CN cannot be used as solvents for solution IR spectra due to their strong absorption bands in the region 1550–1300 cm^{-1}.
(32) Tanaka, K.; Honjo, M.; Tanaka, T. *Inorg. Chem.* **1985**, *24*, 2662.

This difference may be also associated with the difference in the active sites of both electrodes.

Acknowledgment. We are indebted to Dr. Masami Nakamoto, Osaka Municipal Technical Research Institute, for assistance with the FT-IR measurements.

(33) The electrochemical reduction of NO_2^- by the $[Mo_2Fe_6S_8]$/GC at −1.00 V was too slow to analyze the reaction products.

Registry No. DMF, 68-12-2; NO_3^-, 14797-55-8; NO_2^-, 14797-65-0; $(Bu_4N)_4[MoFe_3S_4(SPh)_3(O_2C_6Cl_4)]_2$, 134817-97-3; C, 7440-44-0; NH_3, 7664-41-7; N_2, 7727-37-9; NO, 10102-43-9; $(Bu_4N)_3[Mo_2Fe_6S_8(SPh)_9]$, 68197-68-2; $NaNO_3$, 7631-99-4; $NaNO_2$, 7632-00-0; N_2O, 10024-97-2; Bu_4NBr, 1643-19-2; H_2, 1333-74-0; NH_2OH, 7803-49-8; Bu_4NNO_3, 1941-27-1; CD_3CN, 2206-26-0; CH_3CN, 75-05-8; $(Bu_4N)_2[MoF_3S_4(SPh)_3(O_2C_6Cl_4)(CD_3CN)]$, 134847-22-6.

Contribution from the Institute for Inorganic Chemistry, University of Witten/Herdecke, Stockumer Strasse 10, 5810 Witten, FRG

Volume Profile Analysis of the Formation and Dissociation of Carboxymyoglobin. Comparison with the Corresponding Oxymyoglobin System

Hans-Dieter Projahn and Rudi van Eldik*

Received March 13, 1991

The effect of pressure on the decarbonylation kinetics of carboxymyoglobin was studied by using stopped-flow techniques. The corresponding volume of activation is $\Delta V^{\ddagger}_{off} = -3.8 \pm 1.6$ cm^3 mol^{-1}. The reaction volume was calculated by using pressure-dependent k_{on} values reported in an earlier study to be -4.1 ± 0.8 cm^3 mol^{-1}. It was also measured directly from the pressure dependence of the equilibrium constant, which resulted in a reaction volume of -3.0 ± 0.6 cm^3 mol^{-1}. A comparison of the volume profiles for the reactions of myoglobin with CO and O_2 reveals that the reactions proceed according to two different mechanisms. Bond formation is rate-determining for CO, whereas entry into the protein is rate-determining for O_2. The results are compared to related studies reported in the literature.

Introduction

In recent years the application of high-pressure kinetic techniques has significantly assisted the mechanistic interpretation of reactions in inorganic and organometallic chemistry.[1-3] High-pressure techniques have also been applied to the study of biochemical and bioinorganic systems.[2,4] In this respect the interest in reactions of small molecules (isonitriles, CO, NO, O_2) with the oxygen transport protein myoglobin has increased in recent years. Various methods have been applied to this system in an effort to improve the understanding of the functional reaction paths of this protein, viz. flash photolysis,[5-7] flash photolysis at low temperatures,[8-10] X-ray diffraction,[11-16] neutron diffraction,[17,18] IR/Raman spectroscopy,[9,19,20] cyclic voltammetry,[21] ^{1}H NMR spectroscopy,[21-26] and protein engineering.[27-30] It is commonly accepted that the mechanisms of binding are totally different for oxygen and carbon monoxide. These reactions show different activation barriers (with different conformational states) and different rate-determining steps.[9,29-34] In two recent studies[35,36] we have investigated the reactions of O_2, CO, and isonitriles with myoglobin and some model compounds via the application of high-pressure techniques. A volume profile treatment for the formation and dissociation of oxymyoglobin enabled us to comment

(1) van Eldik, R.; Asano, T.; le Noble, W. J. *Chem. Rev.* **1989**, *89*, 549.
(2) van Eldik, R., Ed *Inorganic High Pressure Chemistry: Kinetics and Mechanisms*; Elsevier; Amsterdam, 1986.
(3) Kotowski, M.; van Eldik, R. *Coord. Chem. Rev.* **1989**, *93*, 19.
(4) Weber, G. In *High Pressure and Biochemistry*; van Eldik, R., Jonas, J., Eds.; NATO ASI Series, Series C, No. 197; Kluwer: Boston, 1987; p 401.
(5) Jongeward, K. A.; Magde, D.; Taube, D. J.; Marsters, J. C.; Traylor, T. G.; Sharma, V. S. *J. Am. Chem. Soc.* **1988**, *110*, 1380.
(6) Ainsworth, S.; Gibson, Q. H. *Nature* **1957**, *180*, 1416.
(7) Hasinoff, B. B. *Biochemistry* **1974**, *13*, 311.
(8) Beece, D.; Eisenstein, L.; Frauenfelder, H.; Good, D.; Marden, M. C.; Reinisch, L.; Reynolds, A. H.; Sorensen, L. B.; Yue, K. T. *Biochemistry* **1980**, *19*, 5147.
(9) Frauenfelder, H.; Alberding, N. A.; Ansari, A.; Braunstein, D.; Cowen, B. R.; Hong, M. K.; Iben, I. E. T.; Johnson, J. B.; Luck, S.; Marden, M. C.; Mourant, J. R.; Ormos, P.; Reinisch, L.; Scholl, R.; Schulte, A.; Shyamsunder, E.; Sorensen, L. B.; Steinbach, P. J.; Xie, A.; Young, R. D.; Yue, K. T. *J. Phys. Chem.* **1990**, *94*, 1024.
(10) Doster, W.; Beece, D.; Browne, S. F.; DiIorio, E. E.; Eisenstein, L.; Frauenfelder, H.; Reinisch, L.; Shyamsunder, E.; Winterhalter, K. H.; Yue, K. F. *Biochemistry* **1982**, *21*, 4831.
(11) Evans, S. V.; Brayer, G. D. *J. Biol. Chem.* **1988**, *263*, 4263.
(12) Ringe, D.; Petsko, G. A.; Kerr, D. E.; Ortiz de Montellano, P. R. *Biochemistry* **1984**, *23*, 2.
(13) Takano, T. *J. Mol. Biol.* **1977**, *110*, 537.
(14) Takano, T. *J. Mol. Biol.* **1977**, *110*, 569.
(15) Phillips, S. E. V. *J. Mol. Biol.* **1980**, *142*, 531.
(16) Kuriyan, J.; Wilz, S.; Karplus, M.; Petsko, G. A. *J. Mol. Biol.* **1986**, *192*, 133.
(17) Phillips, S. E. V.; Schoenborn, B. P. *Nature* **1981**, *292*, 81.
(18) Hanson, J. C.; Schoenborn, B. P. *J. Mol. Biol.* **1981**, *153*, 117.
(19) Morikis, D.; Sage, J. T.; Rizos, A. K.; Champion, P. M. *J. Am. Chem. Soc.* **1988**, *110*, 6341.
(20) Loehr, T. M. Oxygen Binding by the Metalloproteins Hemerythrin, Hemocyanin, and Hemoglobin. In *Oxygen Complexes and Oxygen Activation by Transition Metals*; Martell, A. E., Sawyer, D. T., Eds.; Plenum Press: New York, 1988.
(21) King, B. C.; Hawkridge, F. M. *Talanta* **1989**, *36*, 331.
(22) Lecomte, J. T. J.; La Mar, G. N. *Biochemistry* **1985**, *24*, 7488.
(23) Kottlam, J.; Case, D. A. *J. Am. Chem. Soc.* **1988**, *110*, 7690.
(24) Reisberg, P. I.; Olson, J. S. *J. Biol. Chem.* **1980**, *225*, 4151.
(25) Srajer, V.; Reinisch, L.; Champion, P. M. *J. Am. Chem. Soc.* **1988**, *110*, 6656.
(26) Waleh, A.; Loew, G. H. *J. Am. Chem. Soc.* **1982**, *104*, 2346.
(27) Nagai, K.; Luisi, B. *Nature* **1987**, *329*, 858.
(28) Olson, J. S.; Mathews, A. J.; Rohlfs, R. J.; Springer, B. A.; Egeberg, K. A.; Sligar, S. G.; Tame, J.; Renaud, J.-P.; Nagai, K. *Nature* **1988**, *336*, 265.
(29) Springer, B. A.; Egeberg, K. D.; Sligar, S. G.; Rohlfs, R. J.; Mathews, A. J.; Olson, J. S. *J. Biol. Chem.* **1989**, *264*, 3057.
(30) Springer, B. A.; Sligar, S. G. *Proc. Natl. Acad. Sci. U.S.A.* **1987**, *84*, 8961.
(31) Adachi, S.; Morishima, I. *J. Biol. Chem.* **1989**, *264*, 19896.
(32) Plonka, A. *Chem. Phys. Lett.* **1988**, *151*, 466.
(33) Gibson, Q. H.; Olson, J. S.; McKinnie, R. E.; Rohlfs, R. J. *J. Biol. Chem.* **1986**, *261*, 10228.
(34) Rohlfs, R. J.; Olson, J. S.; Gibson, Q. H. *J. Biol. Chem.* **1988**, *263*, 1803.
(35) Projahn, H.-D.; Dreher, C.; van Eldik, R. *J. Am. Chem. Soc.* **1990**, *112*, 17.
(36) Taube, D. J.; Projahn, H.-D.; van Eldik, R.; Magde, D.; Traylor, T. G. *J. Am. Chem. Soc.* **1990**, *112*, 6880.

0020-1669/91/1330-3288$02.50/0